# Steam reforming of ethanol over Ni/$MgAl_2O_4$ catalysts

Alessandro Di Michele[a], Anna Dell'Angelo[b], Antonio Tripodi[b], Elnaz Bahadori[b], Felipe Sànchez[c], Davide Motta[c], Nikolaos Dimitratos[c], Ilenia Rossetti[b] and Gianguido Ramis[d,*]

[a] Dip. Fisica e Geologia, Università degli Studi di Perugia, Via Pascoli, 06123, Perugia

[b] Chemical Plants and Industrial Chemistry Group, Dip. Chimica, Università degli Studi di Milano, INSTM Unit Milano-Università and CNR-ISTM, via C. Golgi, 19, I-20133 Milano

[c] Cardiff Catalysis Institute, School of Chemistry, Cardiff University, Main Building, Park Place, Cardiff, CF103AT, UK. Cardiff University

[d] Dip. di Ingegneria Civile, Chimica e Ambientale, Università degli Studi di Genova and INSTM Unit Genova, via all'Opera Pia 15A, Genoa, Italy

## Abstract

Hydrogen is considered one of the most promising energy vectors in order to match the current energy and environmental issues. Bioethanol steam reforming is a sound opportunity and close to the industrialization considering an integrated biorefinery concept. $MgAl_2O_4$ was selected as a stable support, with improved activity, selectivity and stability due to negligible acidity. Increasing the Ni loading from 1.5 to 10 wt% over $MgAl_2O_4$ improved the conversion of ethanol as well as the yield of hydrogen, while the carbon deposition and yield of byproducts decreased.

Small acidity characterised the samples, attributed exclusively to the Ni active phase. This prevented extensive catalyst coking due to ethylene formation and subsequent

* Corresponding author: gianguidoramis@unige.it

polymerisation. Consequently, small coke amount was found on the spent catalysts, mainly amorphous, allowing rather easy regeneration.

DRIFT analysis of adsorbed ethanol at variable temperature evidenced the intermediates of reaction and their evolution with temperature, allowing to suggest the main reaction paths. Acetaldehyde was found as intermediate, rapidly evolving to reformate. Among the possible evolution paths of acetaldehyde, the oxidation to acetate and carbonate species (likely stabilised by the support) was preferred with respect to decomposition to methane and CO. This is reflected in the products distribution evidenced through activity testing.

*Keywords:* Hydrogen; Ethylene; Ni catalysts; Bioethanol conversion to chemicals; Steam reforming.

## 1 - Introduction

Increasing attention is focused on hydrogen as a clean energy vector, because its oxidation is highly exothermal and the only product is water [1]. Despite the huge potential benefits, the use of hydrogen is currently limited by the insufficient capacity of hydrogen storage technologies and by the safety issues related with its storage and transportation under mild conditions [2]. Furthermore, nowadays 47% of global hydrogen is produced from natural gas, 30% from oil, 19% from coal and the remaining fraction via water electrolysis [3]; therefore, *ca*. 96% of hydrogen derives from the conversion of fossil resources, which means a net co-production of $CO_2$. New sources and new processes are needed to produce hydrogen in a sustainable way.

Ethanol steam reforming (ESR) has received considerable attention, because ethanol is mainly obtained by renewable sources [4], it is simple to store, handle and transport because of its low volatility and toxicity [5]. This process could be industrially advantageous, ideally

yielding 6 moles of $H_2$ per mole of ethanol reacted. A major drawback is the endothermicity of the reaction, so for process intensification the lowest admissible temperature should be searched. In addition, at low temperature (below 500 °C), side reactions that yield alternative products such as acetic acid, acetaldehyde and ethylene are favoured. These byproducts compete for hydrogen atoms, thus lowering the overall $H_2$ yield [6,7] and can also be related to catalyst deactivation.

It is well known that both the active phase and the support play a key role in determining the productivity and selectivity of the reaction, because different catalysts induce different pathways for $H_2$ production [5,8,9]. Several metal-based catalysts [4,10-17] have been proposed for the steam reforming of alcohols. Nickel is particularly attractive because of its high activity and selectivity in breaking C-C bonds and its lower cost if compared with noble metals. It also catalyzes the water-gas shift reaction [18,19], improving $H_2$ yield and its subsequent purification from CO. However, other challenges related to metal sintering and coke deposition are still open. From these points of view, the choice of the support is crucial. Indeed, the cooperation between the support and the metal is fundamental to stabilize the active phase, increase its dispersion and decrease the rate of coke formation [20-22].

The general reaction scheme is the following:

$$CH_3CH_2OH_{(g)} + H_2O_{(g)} \rightarrow 2\ CO_{(g)} + 4\ H_{2(g)} \qquad \Delta H_{298°C} = +256\ kJ/mol \qquad (1)$$

which couples with the water gas shift (WGS) reaction, which is slightly exothermic

$$2\ CO_{(g)} + 2\ H_2O_{(g)} \leftrightarrows 2\ CO_{2(g)} + 2\ H_{2(g)} \qquad (2)$$

to yield ideally 6 moles of hydrogen per mole of ethanol.

$$CH_3CH_2OH_{(g)} + 3\ H_2O_{(g)} \rightarrow 2\ CO_{2(g)} + 6\ H_{2(g)} \qquad \Delta H_{298°C} = +174 kJ/mol \qquad (3)$$

However, these reactions are not particularly descriptive of the real steam reforming process, which actually occurs through various intermediates. The possible reactions through which ethanol reforming can occur, individually or concurrently, are very numerous and depend on catalyst formulation [22-24]. The main ones are the following:

$$C_2H_5OH_{(g)} \rightarrow CO_{(g)} + CH_{4(g)} + H_{2(g)}, \qquad \Delta H^0_{298} = 49\ kJ/mol \qquad (4)$$

$$C_2H_5OH_{(g)} \leftrightarrows H_{2(g)} + CH_3CHO_{(g)}, \qquad \Delta H^0_{298} = 69\ kJ/mol \qquad (5)$$

$$CH_3CHO_{(g)} \rightarrow CH_{4(g)} + CO_{(g)}, \qquad \Delta H^0_{298} = -19\ kJ/mol \qquad (6)$$

$$CH_3CHO_{(g)} \rightarrow \tfrac{1}{2}\ CH_3COCH_{3(g)} + \tfrac{1}{2}\ CO_{(g)} + \tfrac{1}{2}\ H_{2(g)}, \qquad \Delta H^0_{298} = 2.8\ kJ/mol \qquad (7)$$

$$C_2H_5OH_{(g)} \leftrightarrows C_2H_{4(g)} + H_2O_{(g)}, \qquad \Delta H^0_{298} = 45\ kJ/mol \qquad (8)$$

$$CO_{(g)} + 3H_{2(g)} \leftrightarrows CH_{4(g)} + H_2O_{(g)}, \qquad \Delta H^0_{298} = -205\ kJ/mol \qquad (9)$$

$$2CO_{(g)} \leftrightarrows C_{(s)} + CO_{2(g)}, \qquad \Delta H^0_{298} = -171.5\ kJ/mol \qquad (10)$$

$$C_2H_{4(g)} \rightarrow\rightarrow\rightarrow\rightarrow \text{Coke} \qquad (11)$$

In this study, $MgAl_2O_4$ was employed as support for Ni-based catalysts. Mg–Al mixed oxide supported Ni catalysts showed high activity in terms of $H_2$ productivity and catalyst stability compared to nickel catalysts supported on pure oxides [25]. $MgAl_2O_4$ was chosen due to the following factors: (i) it is a slightly basic material, (ii) it exhibits moderate acidic and basic site strength and density, (iii) it limits the promotion of reactions 8 and 11, thus, minimises coke formation and therefore enhances catalyst stability [26]. For example, Katheria et al. investigated this spinel as support for nickel during methane steam reforming, revealing a strong dependence of catalyst activity on the synthetic conditions. In particular, an increase of methane conversion was attributed to a higher metal dispersion and lower active metal

particle size of the catalyst obtained by the reported washcoating synthesis technique on FeCr-alloy [27].

Therefore, in this manuscript we investigated a series of Ni/$MgAl_2O_4$ catalysts with different Ni loading and prepared with an ultrasound assisted technique to achieve high surface area and, thus, metal dispersion. Ethanol Steam Reforming (ESR) tests were carried out in a continuous bench scale reactor operated at 625 °C, 500 °C and 400 °C, especially focusing on low temperatures for this application, for process intensification. A critical value of ethanol/water molar feed ratio was used (1:3 mol/mol) as stressing condition to monitor catalyst deactivation. Rival data in the literature (vide infra) are indeed collected at higher water/ethanol ratio. The effect of metal loading on activity and hydrogen selectivity was investigated, together with possible deactivating phenomena. Finally, DRIFTS analysis allowed to evidence the intermediates and their evolution with reaction temperature as a support to discriminate between different reaction paths.

## 2 - Experimental Section

### *2.1 - Catalysts preparation*

$MgAl_2O_4$ was prepared as follows. 150 ml of a solution of 1.9 M HCl and 16 g of CTABr (Trimethylcetylammonium bromide) were mixed under magnetic stirring at 40 °C to a solution of 300 ml of ethanol in which 123 g of aluminium isopropoxide and 13 g of $Mg(OCH_2CH_3)_2$ were dissolved. Part of the $MgAl_2O_4$ was dried at 110 °C and calcined at 650 °C for 3h under static air. The active phase was added to the support through the co-precipitation method under high power ultrasound irradiation using an Ultrasonic processors VC750 Sonics and Materials, 20 KHz with a diameter tip of 13 mm. For the synthesis 100 mL of a $NH_4HCO_3$ 1M solution were dropped, under ultrasound irradiation for 1 h A at 50% of Amplitude, to a diluted solution of nickel acetate-$MgAl_2O_4$, in the desired concentration in order to obtain 1.5 wt% Ni/$MgAl_2O_4$ (M1), 5 wt% Ni/$MgAl_2O_4$ (M2) and 10 wt% Ni/$MgAl_2O_4$ (M3) loading. The precipitates were dried and calcined at 500 °C for 3 h under static air.

## *2.2 - Catalysts characterization*

XRD data were collected at ambient temperature with a PANanalytical X'PertPRO X-ray diffractometer using Cu Kα radiation and operated at 40 kV and 30 mA. X-ray diffraction patterns were recorded between 2θ = 10-80° at a step size of 0.017°. The crystallite size was calculated by the Scherrer equation:

$$D(nm) = \frac{K\lambda}{L\cos\theta}$$

Where *D* is the mean size of the crystalline domains, *K* is a dimensionless shape factor, with a typical value of about 0.9, *λ* is the X-ray wavelength, Cu Kα radiation =0.154059 nm; *L* is the line broadening at half the maximum intensity (FWHM), *θ* is the Bragg angle (in degrees).

X-ray photoelectron spectra (XPS) were recorded though a K-Alpha™+ X-ray Photoelectron Spectrometer (XPS) System using a monochromatic Al Kα X-ray source. X-ray source (75-150W) and analyzer pass energies were 160 eV (for survey scans) or 40 eV (for detailed scans).

The morphology was examined by Field Emission Gun Electron Scanning Microscopy (FE-SEM) through a LEO 1525 ZEISS instrument. Elemental composition was determined using a combined Bruker Quantax EDS. Transmission Electron Micrographs (TEM) were collected on the fresh and spent samples using a Philips 208 Transmission Electron Microscope. The samples were prepared by putting one drop of an ethanol dispersion of the catalysts on a copper grid, pre-coated with a Formvar film and dried in air.

Adsorption/desorption isotherms were collected at liquid nitrogen temperature (-196 °C) using a Micromeritics ASAP 2020 instrument. Surface area was calculated on the basis of

the Brunauer, Emmet and Teller equation (BET), while the pores size distribution was determined by the BJH method, applied to the $N_2$ desorption branch of the isotherm. Prior to the analysis the samples were outgassed at 300 °C for 24 hours.

$NH_3$-TPD was carried out using a Quantachrome ChemBET TPR/TPD chemisorption analyser with a TCD, following a method including four main steps. During the pre-treatment, 50 mg of sample were heated at 15 °C/min up to 130 °C during 1 h in a flow of He (80ml/min), followed by adsorption of ammonia at room temperature for 20 min to ensure saturation. Then, the physisorbed ammonia was removed at 100 °C (1h, 15 °C/min) in He flow. The last step was the desorption of chemisorbed ammonia by heating up to 800 °C (at 10 °C/min) in He monitoring the desorption with a TCD at attenuation 1 and current 180 mV.

Temperature Programmed Reduction (TPR) measurements were performed by placing the catalyst in a quartz reactor and heating by 10 °C/min from r.t. to 800 °C in a 10 vol% $H_2/N_2$ gas stream flowing at 40 ml/min. TPO (Temperature Programmed Oxidation) measurements were performed placing the spent catalysts in a quartz reactor. The temperature was increased at a rate of 10 °C/min from r.t. to 800 °C in a 10 vol% $O_2$/He gas stream (40ml/min) and the data obtained were elaborated by the Origin Pro 8.5 software.

DRIFTS analysis was performed with a Bruker Tensor 27 spectrometer fitted with a HgCdTe (MCT) detector, a Harrick Praying Mantis HVC-DRP-4 cell equipped with two ZnSe windows and operated with OPUS software. The DRIFTS cell included gas inlet and outlet ports that have the capability to heat and cool the sample. This technique was applied to study the interaction of ethanol with the catalysts. The sample was heated to 120 °C under 20 ml/min of $N_2$ for 30 minutes, in order to eliminate any physisorbed molecule on the material, after that time an IR background spectra was collected. Afterwards, ethanol was supplied until saturation (around 20 min). Then $N_2$ flow was continued until adsorbed ethanol was evacuated. When the DRIFT spectra were not changing, the temperature was increased to 200 °C for 30 min and the resulting spectra recorded. This last step was repeated for other

temperatures (*i.e*. 300, 400 and 500 °C). The data are reported as absorbance. Each spectrum represents an average of 64 scans collected with a spectral resolution of 2 $cm^{-1}$. In the reported spectra, a positive peak intensity indicates an increase of population of a given species, whereas a negative deflection shows a loss of the same.

Micro-Raman sampling was made by an OLYMPUS microscope (model BX40) connected to an ISA Jobin– Yvon model TRIAX320 single monochromator, with a resolution of 1 $cm^{-1}$. The source of excitation was a Melles Griot 25LHP925 He–Ne laser that was used in single line excitation mode at l = 632.8 nm. The power focused on the samples was always less than 2 mW. The scattered Raman photons were detected by a liquid-nitrogen cooled charge coupled device (CCD, Jobin–Yvon mod. Spectrum One).

### *2.3 - Activity testing*

Activity tests were run through a continuous micropilot plant constituted by an Incoloy 800 downflow reactor (internal diameter 0.9 cm and length 40 cm), heated by an electric oven. The reactor temperature was controlled by an Eurotherm 3204 TIC. The catalysts were pressed, ground and sieved into 0.15–0.25 mm particles and 0.5 g of catalyst were loaded into the reactor after dilution 1:3 (vol/vol) with SiC of the same particle size. Catalyst activation was accomplished by feeding 50 ml/min of a 20 vol% $H_2/N_2$ gas mixture at 625 °C for 1h. During activity testing 0.017 ml/min of a 3:1 (mol/mol) water/ethanol liquid mixture were fed to the reactor by means of a Hitachi, mod. L7100, HPLC pump, added with 50 ml/min of $N_2$, used as internal standard, and 174 ml/min of He. The liquid mixture was vaporized in the hot inlet of the reactor before reaching the catalyst bed. Such dilution of the feed stream allowed to keep the reactants mixture in the vapour phase even at zero conversion at the reactor outlet. The activity tests were carried out at atmospheric pressure, with a Gas Hourly Space Velocity (GHSV) of 2,700 $h^{-1}$ (referred to the water/ethanol gaseous mixture), corresponding to *ca*. 1,000 g min/mol, at 625, 500 and 400 °C. The testing

sequence was programmed from the highest temperature to the lowest, in order to avoid possible deactivation by coking of the samples and structural changes of the catalyst. The test duration does not allow to fully assess stability, however, as for an internal comparison, the monitoring of coke accumulation for a fixed reaction time is still a valid measure of catalyst stability. Therefore, the testing sequence was on purpose from the highest temperature to the lowest in order to progressively accumulate coke (when relevant), accumulation that is favoured at low temperature since the carbon gasification activity is poor.

Analysis of out-flowing gas was performed by a gas chromatograph (Agilent, mod. 7980A) equipped with two columns connected in series (Poraplot Q and Molecular Sieves) with a thermal conductivity detector (TCD), properly calibrated for the detection of ethanol, acetaldehyde, acetone, acetic acid, water, ethylene, CO, $CO_2$ and $H_2$. Repeated analyses of the effluent gas were carried out every hour and the duration of every test at each temperature was 8 h-on-stream to reach steady-state conditions. The raw data, expressed as mol/min of each species outflowing from the reactor, have been elaborated as detailed elsewhere [26,28]. Material balance on C-containing products was used as first hand indicator to evaluate coke deposition.

## 3 - Results and Discussion

### *3.1 - Catalyst characterization*

X-ray diffraction patterns of the fresh catalysts are shown in Figure 1. In all the cases, broad diffraction peaks corresponding to $MgAl_2O_4$ ($2\theta$ = 19.03, 31.3, 36.8, 44.8, 55.6, 59.4 and 65.2 degrees), NiO ($2\theta$ = 43.3, 37.3, 62.9 degrees) and metallic Ni ($2\theta$ = 77 degrees) were detected [28]. The Figure shows well-defined and large peaks, which demonstrate well-

dispersed particles with uniform size and good crystallinity. Peak broadening testifies the presence of very small crystal size, which is important for the present application to ensure Ni resistance towards the accumulation of subsurface carbides, which are precursors of C nanotubes [29-35].

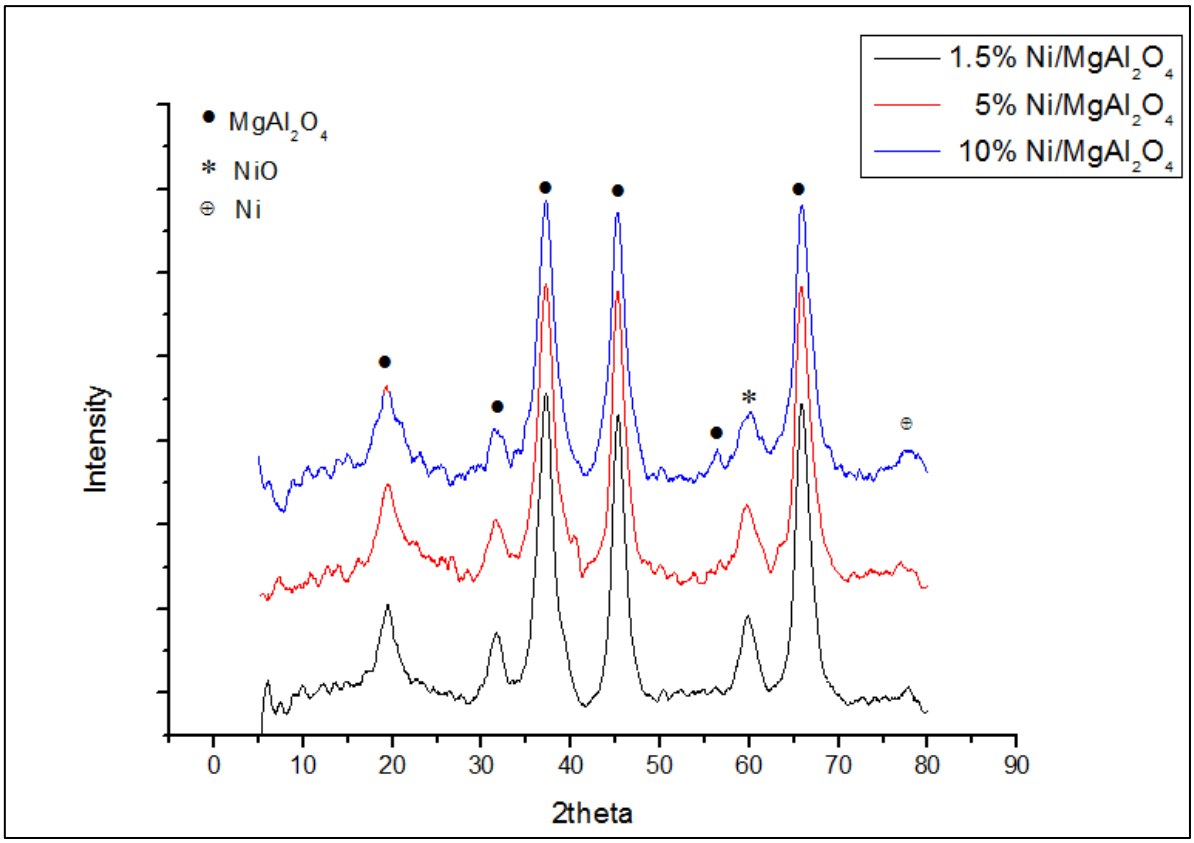


**Figure 1.** Diffraction patterns of fresh catalysts.

Table 1 shows the crystallite size (D), calculated using the Scherrer equation.

**Table 1:** Crystal size calculated through the Scherrer equation and specific surface area (SSA) from BET analysis.

| Sample | Particles | 2θ | FWHM | D (nm) | SSA ($m^2/g$) |
|---|---|---|---|---|---|
| 1.5% Ni fresh | Ni | 76 | 0.4 | 24.9 | 238 |
| | NiO | 63 | 1.6 | 5.8 | |
| | | | | | |
| 5% Ni fresh | Ni | 76 | 0.4 | 24.9 | 228 |
| | NiO | 63 | 1.5 | 6.1 | |
| | | | | | |
| 10% Ni fresh | Ni | 76 | 0.3 | 33.2 | 228 |
| | NiO | 63 | 1.4 | 6.6 | |

The specific surface area of the samples is also shown in Table 1. The impregnation leads to a very slight decrease of surface area while increasing Ni loading (238-228 $m^2/g$). Small crystal size and high surface area are formed thanks to the optimized preparation procedure, assisted by ultrasounds. The Ni particle size does not vary very much with increasing Ni loading. It remains almost unchanged when passing from 1.5 to 5 wt%, whereas it increases from *ca.* 25 to *ca.* 33 nm when further doubling the Ni loading. The residual NiO particles are even smaller with slightly increasing size with increasing metal amount. This supports the ability of the support and the preparation method in keeping sufficiently dispersed the active phase, which does not coalesce in bigger particles event at highly increasing loading. The X-ray photoelectron spectroscopy (XPS) results are summarized in Table 2 as relative atomic percentage. The results on the fresh samples show a linear decrease of NiO with a decrease of nominal Ni wt% and at the same time an increase of $Ni(OH)_2$ on the surface. Figure 2 shows the deconvolution of $Ni2p_{3/2}$ for all the samples. Ni2p peak has significantly

split spin-orbit components and Ni metal spectrum has a complex shape. In the spectra are visible the specific energy binding ascribable to Ni metal (852.6 eV), NiO(853.7 eV) and $Ni(OH)_2$ (855.6 eV) [36,37].

Different oxidation states of Ni were also visible in the XRD patterns (Fig. 1), in agreement with XPS data. In the 10 wt% $Ni/MgAl_2O_4$ spent sample a low amount of metallic Ni was also present. We observed that the surface composition of the spinel changed for 10 wt% $Ni/MgAl_2O_4$. This could be explained by the substitution of Ni for Mg in the spinel structure. $NiAl_2O_4$ could form predominantly at the surface, so both Ni and Al exposure increases with respect to the sample 5 wt% $Ni/MgAl_2O_4$. The incorporation of Ni in the support surface increases its dispersion even for high metal loading. This is typically desirable to improve resistance to the formation of C nanotubes over Ni particles, as already mentioned above.

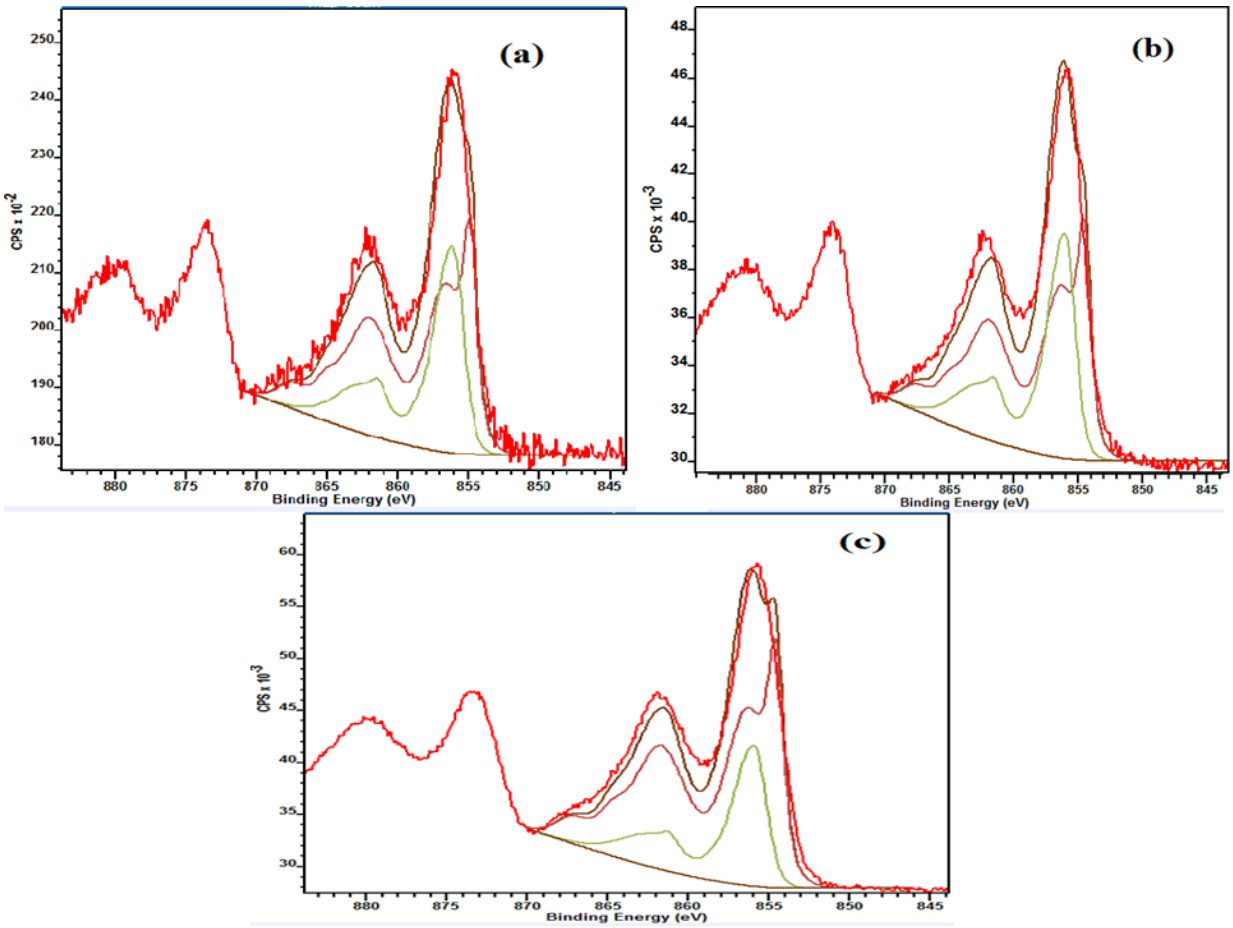

**Figure 2**. XPS spectra deconvolution of $Ni2p_{3/2}$ for catalysts 1.5 wt% **(a),** 5 wt% **(b)** and 10 wt% **(c)** $Ni/MgAl_2O_4$.

**Table 2:** XPS of the fresh catalysts.

| Cat | Name | Pos | FWHM | At% |
|---|---|---|---|---|
| **1.5%Ni** | O 1s | 530.86 | 3.32 | 48.67 |
| | C 1s | 284.86 | 3.01 | 2.4 |
| | Ni 2p | 855.86 | 3.5 | 0.66 |
| | Mg 2s | 88.86 | 4.14 | 13.55 |
| | Al 2p | 74.86 | 2.89 | 34.71 |
| | | | | |
| **5%Ni** | Name | Pos | FWHM | At% |
| | O 1s | 532.08 | 3.32 | 47.27 |
| | C 1s | 285.08 | 3.37 | 2.84 |
| | Ni 2p | 856.08 | 4.11 | 1.14 |
| | Mg 2s | 89.08 | 4.08 | 13.61 |
| | Al 2p | 75.08 | 2.93 | 35.18 |
| | | | | |
| **10%Ni** | Name | Pos | FWHM | At% |
| | O 1s | 531.86 | 3.42 | 43.29 |
| | C 1s | 284.86 | 2.85 | 2.66 |
| | Ni 2p | 855.86 | 4.32 | 3.05 |
| | Mg 2s | 88.86 | 4.13 | 9.22 |
| | Al 2p | 74.86 | 3.09 | 41.78 |

The fresh catalysts were constituted by rather uniform oxide particles, *ca*. 25-45 nm, with a homogeneous distribution of the active phase over it (Fig. 3, 4).

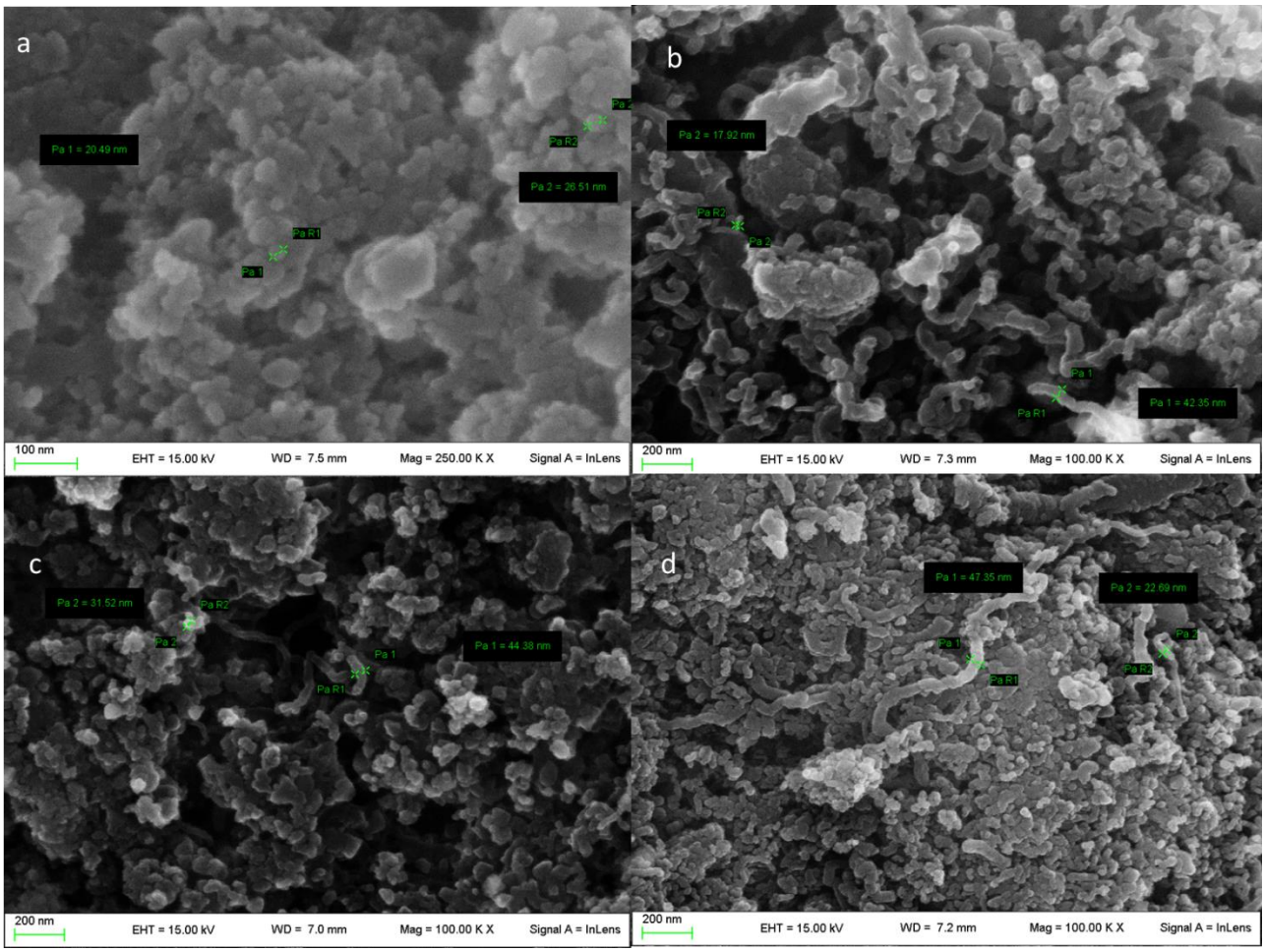


**Figure 3**. FE-SEM images for catalysts Ni/$MgAl_2O_4$ 1.5 wt%, fresh **(a),** 1.5 wt%, after reaction **(b)**, 5 wt% after reaction **(c)** and 10 wt% after reaction **(d)**.

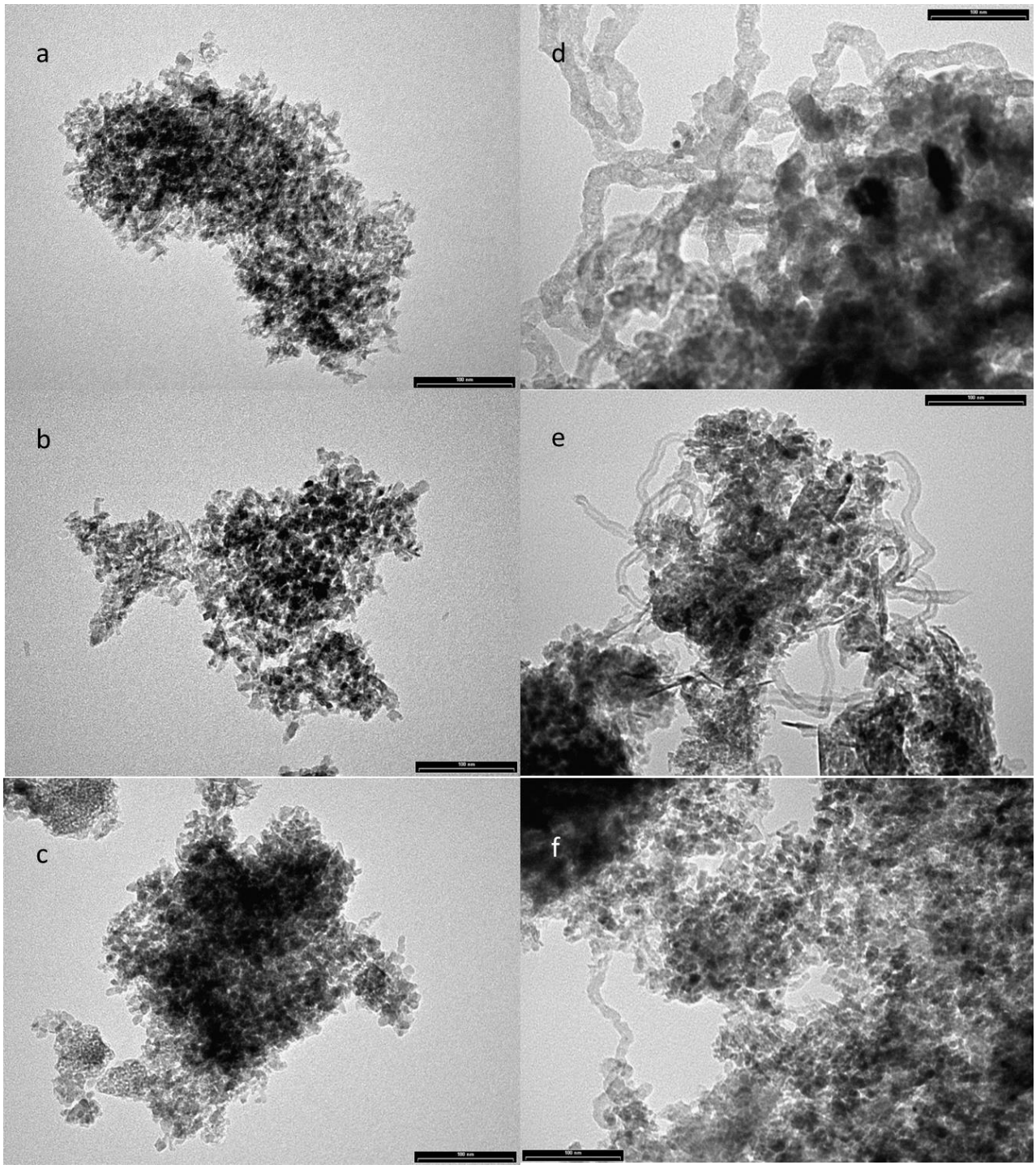


**Figure 4**. TEM images of the catalysts Ni/$MgAl_2O_4$ 1.5 wt%, **(a = fresh, d = spent),** 5 wt% **(b = fresh, e = spent)** and 10 wt% **(c = fresh, f = spent)**.

## *3.2 - Activity tests*

The results of catalytic testing at 625 °C are summarized in Table 3 and Fig. 5. Ethanol conversion was 86 % for sample 1.5wt% Ni, while increased with increasing Ni content.

Indeed, samples 5 wt% Ni and 10 wt% Ni led to full ethanol conversion with the highest $H_2$ productivity. Increasing Ni loading also improved the productivity of $H_2$ due to higher activity for the water gas shift reaction (lower $CO/CO_2$ ratio) and decreased selectivity to $CH_4$ (Fig. 6). Ethylene was observed at the lowest Ni content, only, due to insufficient activity for the further reforming of this intermediate. Low Ni loading is characterized by insufficient activity for C-C bond cleavage, leaving indeed unreacted ethanol and unconverted ethylene.

Sample 1.5 wt% Ni proved also insufficiently stable, since ethanol conversion started decreasing after 450 minutes-on-stream and the selectivity to acetaldehyde increased simultaneously (Fig. 5). On the contrary, samples 5 wt% Ni and 10 wt% Ni were stable for the whole duration of the test, with negligible selectivity to acetaldehyde, confirming the better stability of these samples.

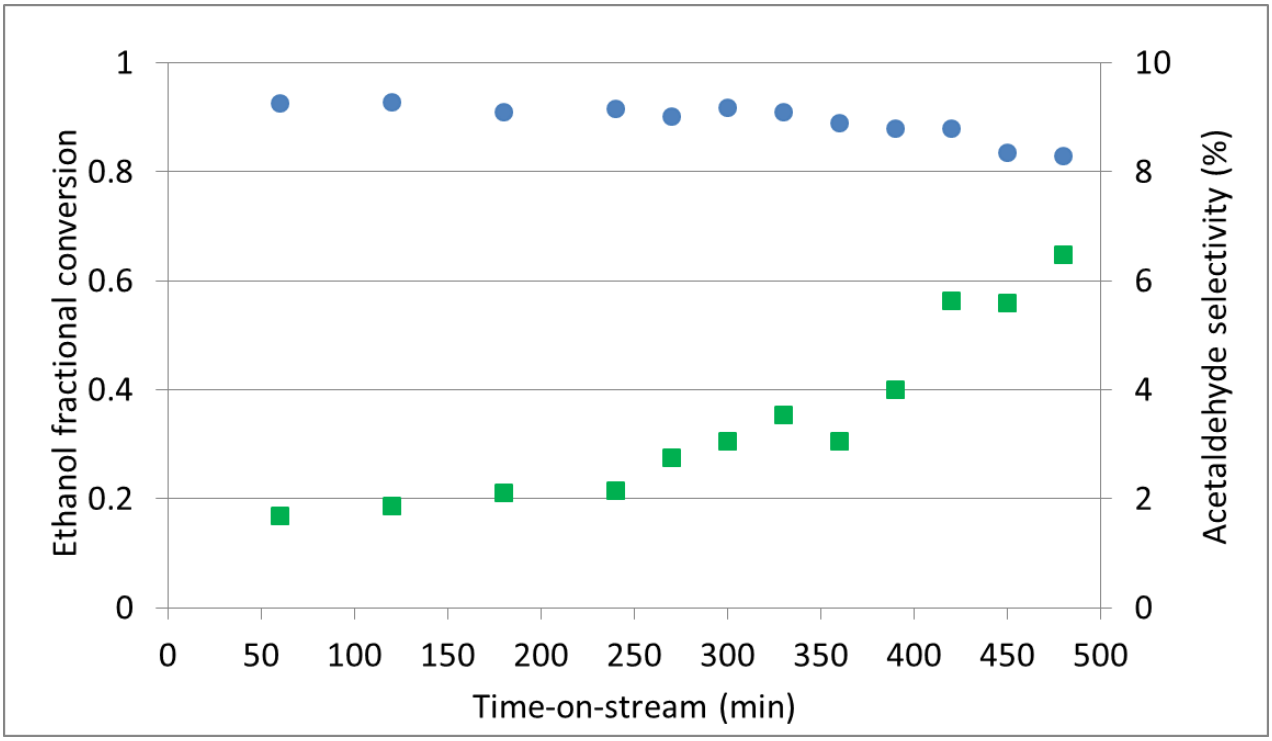


**Figure 5.** Ethanol conversion (blue circles) and acetaldehyde selectivity (green squares) of 1.5% $Ni/MgAl_2O_4$ at 625 °C.

When the catalytic performance of the samples was evaluated at 500 °C the same trend of activity versus Ni loading was confirmed, but the catalysts were generally much less active than at higher temperature (Table 4). A lower $CO/CO_2$ ratio was obtained irrespectively of the sample due to the thermodynamically favored equilibrium of the water gas shift reaction at lower temperature. Catalyst activity at this temperature was insufficient to fully convert byproducts, *e.g.* acetone and acetaldehyde, and, as a matter of fact, ethylene was the main product of the reaction.

A further decrease of the operating temperature, the only sample maintaining a (limited) activity for ESR was 10 wt% Ni (Table 5). The main products were ethylene and acetaldehyde, with a non negligible fraction of acetone, especially at low Ni loading.

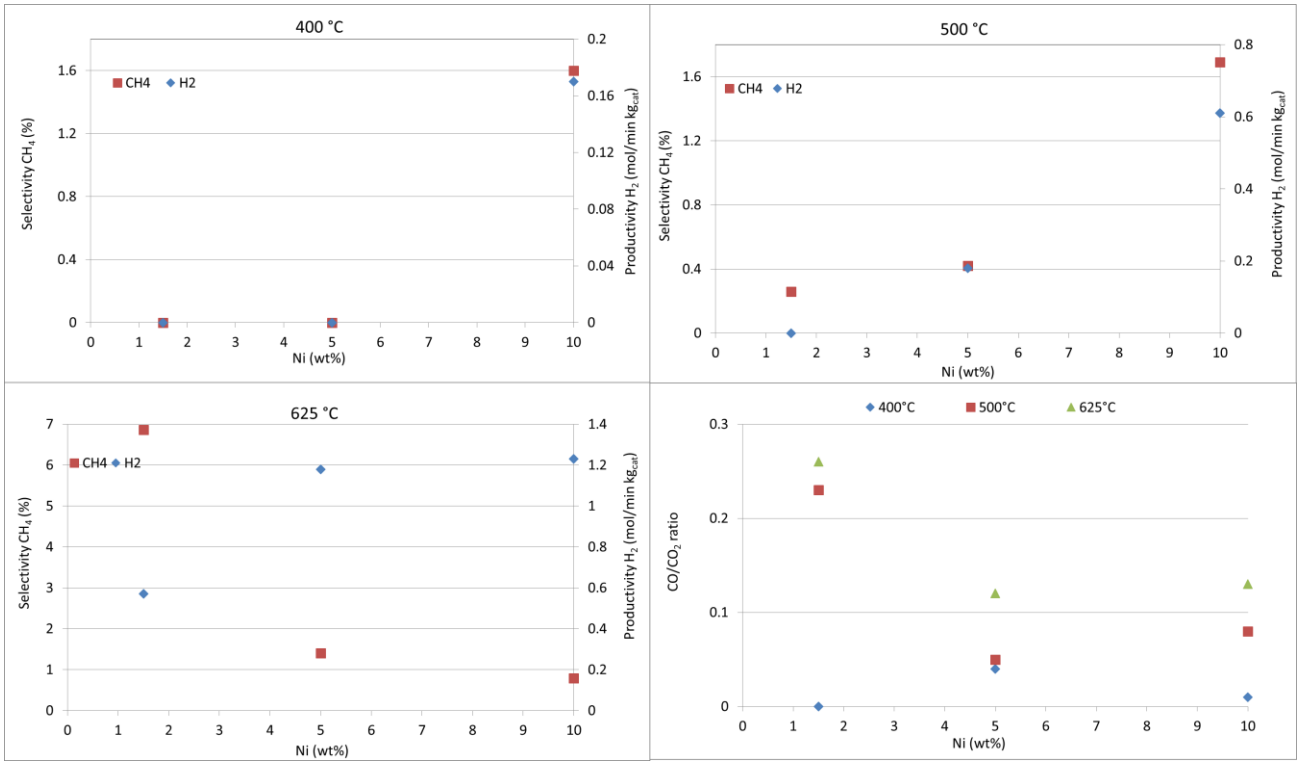


**Figure 6.** Trends of hydrogen productivity, methane selectivity and $CO/CO_2$ ratio at different Ni loading and temperature.

**Table 3**: Results of ESR activity testing at 625 °C.

| | 1.5 wt% Ni | 5 wt% Ni | 10 wt% Ni |
|---|---|---|---|
| $C_2H_5OH$ conversion (%) | 86 ± 3 | 100 | 100 |
| C balance (%) | 107 ± 3 | 93 ± 3 | 98.4 ± 0.7 |
| $H_2$ productivity (mol/min $kg_{cat}$) | 0.57 ± 0.05 | 1.18 ± 0.06 | 1.23 ± 0.04 |
| $CO/CO_2$ | 7.0 ± 0.3 | 1.05 ± 0.12 | 1.18 ± 0.13 |
| Sel. $CH_4$ (%) | 6.9 ± 0.4 | 1.40 ± 0.09 | 0.79 ± 0.02 |
| Sel. $CH_3CHO$ (%) | 2.8 ± 0.8 | 0 ± 0 | 1.7 ± 0.4 |
| Sel. $CH_3COCH_3$ (%) | 2.4 ± 0.6 | 0 ± 0 | 0 ± 0 |
| Sel. $CH_2CH_2$ (%) | 40.8 ± 1.1 | 0 ± 0 | 0 ± 0 |
| Yield $H_2$ (mol $H_{2\ out}$/mol $C_2H_5OH_{in}$) | 1.8 ± 0.2 | 3.8 ± 0.2 | 3.87 ± 0.13 |

**Table 4**: Results of ESR activity testing at 500 °C.

| | 1.5 wt% Ni | 5 wt% Ni | 10 wt% Ni |
|---|---|---|---|
| $C_2H_5OH$ conversion (%) | 100 | 100 | 100 |
| C balance (%) | 90 ± 2 | 85.4 ± 0.2 | 92 ± 2 |
| $H_2$ productivity (mol/min $kg_{cat}$) | 0 ± 0 | 0.181 ± 0.014 | 0.61 ± 0.02 |
| $CO/CO_2$ | 1.0 ± 0.2 | 1.0 ± 0.2 | 1.0 ± 0.2 |
| Sel. $CH_4$ (%) | 0.26 ± 0.02 | 0.42 ± 0.04 | 1.69 ± 0.12 |
| Sel. $CH_3CHO$ (%) | 8.9 ± 0.5 | 2.37 ± 0.07 | 0 ± 0 |
| Sel. $CH_3COCH_3$ (%) | 1.41 ± 0.07 | 2.48 ± 0.07 | 3.2 ± 0.3 |
| Sel. $CH_2CH_2$ (%) | 77 ± 3 | 66.03 ± 0.18 | 41.2 ± 0.9 |
| Yield $H_2$ (mol $H_{2\ out}$/mol $C_2H_5OH_{in}$) | 0 ± 0 | 0.58 ± 0.05 | 1.91 ± 0.06 |

**Table 5**: Results of ESR activity testing at 400 °C.

| | 1.5 wt% Ni | 5 wt% Ni | 10 wt% Ni |
|---|---|---|---|
| $C_2H_5OH$ conversion (%) | 57 ± 4 | 87.67 ± 0.14 | 100 |
| C balance (%) | 95.5 ± 0.8 | 89 ± 6 | 89 ± 3 |
| $H_2$ productivity (mol/min $kg_{cat}$) | 0 ± 0 | 0 ± 0 | 0.169 ± 0.010 |
| $CO/CO_2$ | 0 ± 0 | 1.0 ± 0.5 | 0 ± 0 |
| Sel. $CH_4$ (%) | 0 ± 0 | 0 ± 0 | 1.6 ± 0.3 |
| Sel. $CH_3CHO$ (%) | 4.8 ± 1.0 | 4.8 ± 0.3 | 8.2 ± 0.4 |
| Sel. $CH_3COCH_3$ (%) | 19.3 ± 1.2 | 10.5 ± 1.0 | 2.9 ± 0.9 |
| Sel. $CH_2CH_2$ (%) | 68.0 ± 1.0 | 74 ± 3 | 63.6 ± 1.3 |
| Yield $H_2$ (mol $H_{2\ out}$/mol $C_2H_5OH_{in}$) | 0 ± 0 | 0 ± 0 | 0.53 ± 0.03 |

### *3.3 - TPD of preadsorbed $NH_3$*

In previous studies we have shown the essential role of acidic sites for facilitating the formation of ethylene and affecting hydrogen productivity. The acidity of the catalysts was evaluated and compared by temperature programmed desorption of ammonia ($NH_3$-TPD). The strength of the acid sites was estimated according to the intensity and temperature of the $NH_3$ desorption peak. The acid strength can be classified as weak (150–250 °C), medium (250–420 °C) and strong (420–750 °C) according to the temperature range of ammonia release. Figure 7 shows the results of the analysis. Negligible ammonia adsorption was achieved for the bare support and for sample Ni 1.5 wt%. By contrast, for Ni 5 wt% three desorption peaks were evident at 370, 504 and 660 °C, while for Ni 10 wt% three at 416, 630 and 756 °C indicating the presence of both medium and strong acid sites, with increasing amount and strength with increasing Ni loading (increasing ammonia desorption

temperature and peak intensity). Hence, acidity was mainly ascribed to Ni and not to the basic support. This acidity is the responsible factor of promoting ethanol dehydration to ethylene and the somehow stronger acidity observed at the highest Ni loading can explain the deactivation of the 10 wt% Ni catalyst even at the highest temperature; if C accumulates over Ni particles their activity for ESR and in general for C-C bond cleavage decreases. The increase of acid sites influenced the deposition of carbon which increased proportionally with nickel loading, as shown in the TPO chart (*vide infra*).

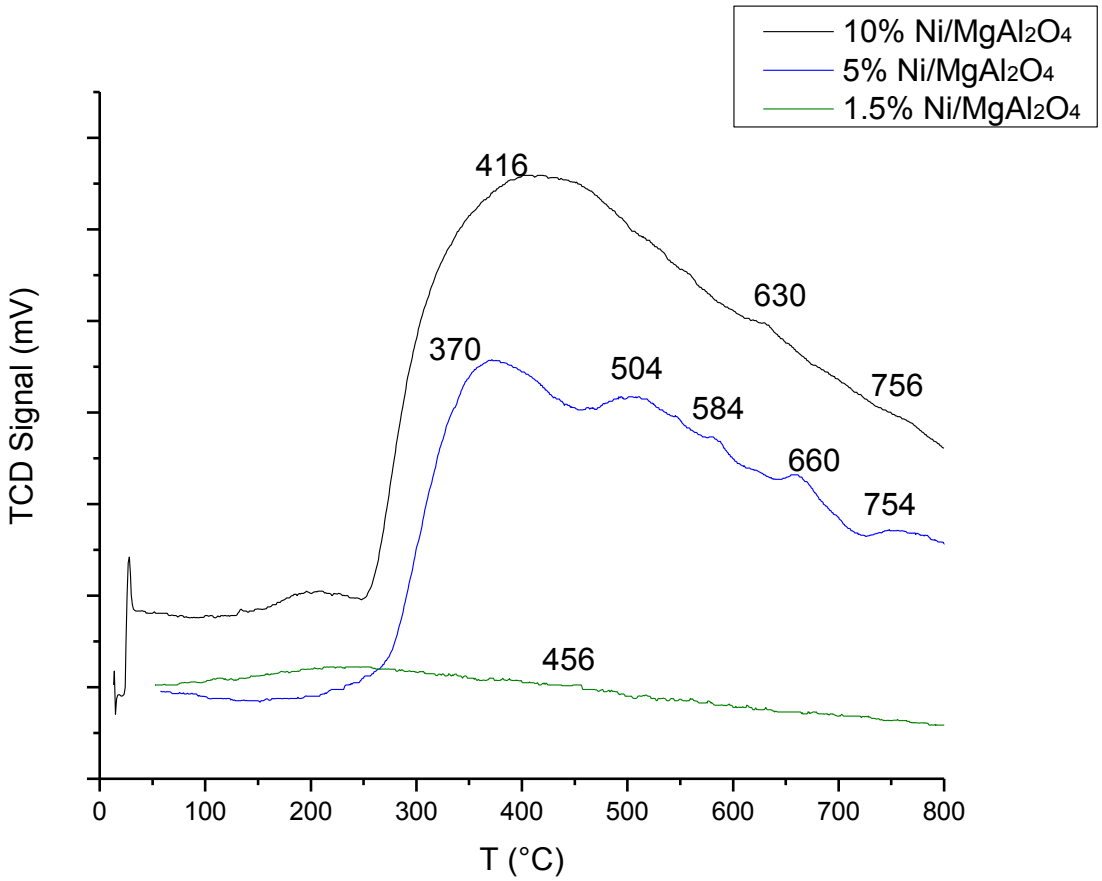


**Figure 7**: $NH_3$-TPD of the different samples. Ni loading increasing from bottom to upper curve.

### *3.4 - DRIFTS Analysis of ethanol adorption/desorption*

To get insight on the possible surface species responsible for the activity and selectivity adsorption/desorption studies of ethanol were carried out in the temperature range 110 - 400 °C. Figure 8 shows the resulting DRIFTS spectra of the samples, which were interpreted on the basis of the relevant literature as for bands assignment [38-40]. The spectra correspond to the adsorption of ethanol at 400 °C. The observed small band at 1249 $cm^{-1}$ corresponds to the OH bending (δ) mode of undissociated adsorbed ethanol. The negative band near 3740 $cm^{-1}$ is due to the interaction of the free surface OH groups with the adsorbed molecules. The sharpness of the latter band and the absence of broad absorption between 3000 and 3500 $cm^{-1}$ indicate that this species should be chemisorbed through the oxygen lone pair, rather than being H bonded. The complex absorption found in the region 2800−2400 $cm^{-1}$ (unusually strong) is associated with this species and is likely due to a Fermi resonance of the overtone of the OH δ vibration mode with the CH stretching (ν), symmetric (s) and asymmetric (as) modes, found at 2967, 2924, and 2879 $cm^{-1}$ ($CH_3$ $\nu_{as}$, $CH_2$ $\nu_{as}$ and $CH_3$ $\nu_s$). At high temperature (Figure 9), some new bands appeared at 1332, 1415, and 1476 $cm^{-1}$ (the last two being very broad). These bands may be assigned to the vibrational modes of acetate species ($CH_3$ δ, OCO $\nu_s$, and OCO $\nu_{as}$, respectively) [41,42], confirming the acetaldehyde formation upon ethanol dehydrogenation as first step of the reforming path.

The broadening of the band at 1476 $cm^{-1}$ and the apparent complexity of both main components suggest that carbonate species, responsible for bands in the same region, should also form. Their appearance is caused by the formation of $CO_2$ derived by the ethanol reforming, which remains adsorbed as carbonate on the basic support used. The shoulder around 1631 $cm^{-1}$ may be assigned to the C-O stretching of acetaldehyde, which may be rapidly oxidized to acetate species. These results are in agreement with the catalytic data

obtained at lower temperature where one of the intermediates detected was acetaldehyde. Often, acetaldehyde is not detected in the products distribution due to its rapid evolution by further oxidation or decomposition to CO and $CH_4$.

DRIFTS experiments also highlighted the formation of acetates, based on the bands at 1332 and 1415 $cm^{-1}$ [43]. The spectral profile of sample 10 wt% Ni (Figure 9) shows a reduction of bands intensity of $CH_x$ during the temperature increase, with a corresponding increase of the carbonate ones. Also, the formation of a shoulder at ca. 1700 $cm^{-1}$, appearing at 300°C and increasing at higher temperature is related to oxidized C species, such as carbonyls and carboxylic groups. This supports the oxidative evolution of acetaldehyde over the present catalysts, rather than its decomposition. It should be underlined that acetaldehyde formation by dehydrogenation of ethanol is catalyzed by Ni active sites, which remain active for this reaction even when possible coke accumulation occurs over it. The C-C bond cleavage, mediated by the same active sites, becomes inactive after encapsulating coking occurs, thus leading to increasing presence of unconverted acetaldehyde in the products distribution. This latter is indeed a fingerprint of the formation of encapsulating coke.

The higher activity of the 10 wt% Ni sample is here testified by the increased intensity of the bands of the more oxidized species (acetates, carbonates) with respect to the $CH_x$ bands.

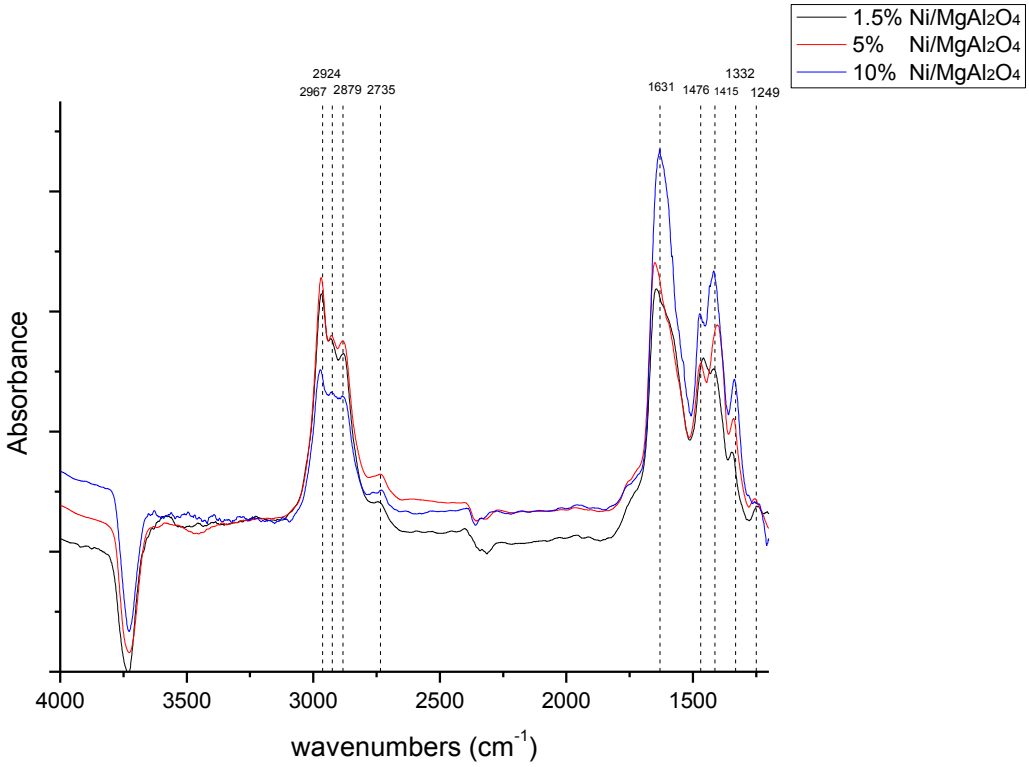


**Figure 8**. DRIFT spectra after adsorption of ethanol at 400 °C.

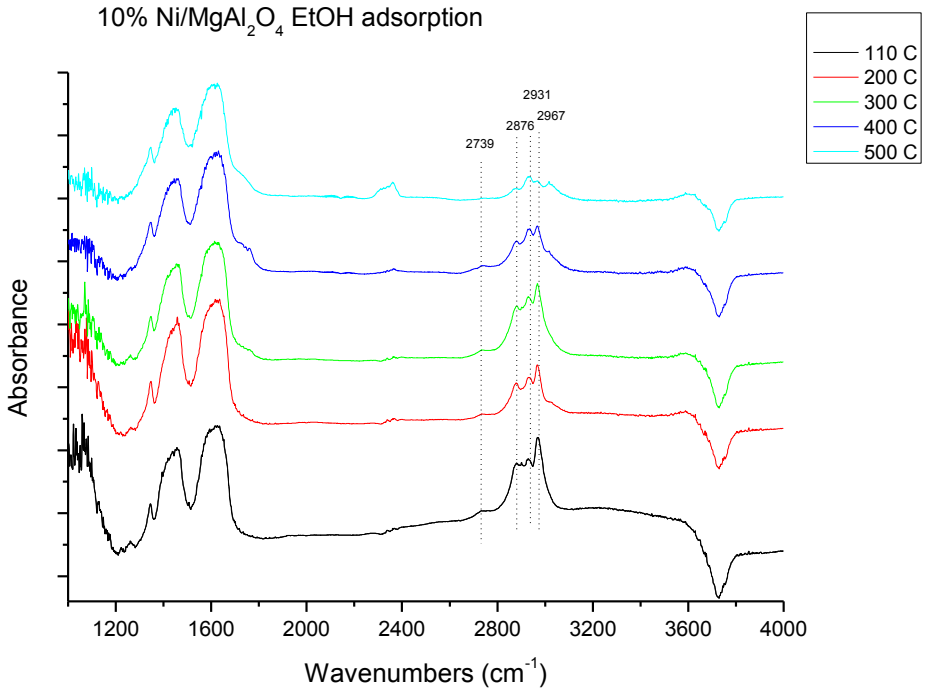


**Figure 9**. DRIFTS spectra of ethanol adsorption on 10 wt% $Ni/MgAl_2O_4$ at different temperature.

### *3.5 - Temperature programmed reduction (TPR)*

Temperature programmed reduction profiles are presented in Figure 10. Each positive peak represents the consumption of $H_2$. The highest is the reduction temperature, the hardest the reducibility of that species. The TPR for 10 wt% Ni/$MgAl_2O_4$ shows a main, broad reduction feature between 300 and 400 °C, representing the reduction of NiO. A small shoulder at higher temperature can represent a fraction of $Ni^{2+}$ as aluminate. The TPR profile of sample 5 wt% Ni presents a peak around 250 °C which suggests the presence of $Ni^{2+}$ species very similar in nature, but in lower amount than 10 wt% Ni, in agreement with XPS data. Additionally, a low temperature peak appeared, due to NiO poorly interacting with the support (for instance bigger particles) and is present also at the lowest Ni loading.

From these data, one can conclude that at the selected activation temperature NiO species are fully reduced to metallic Ni. Very similar NiO species are present in all samples, when the chosen reduction temperature was between 300 and 400 °C. These are accompanied by low temperature reduction features in the case of 1.5 wt% Ni and 5 wt% Ni, almost undetectable for the highest Ni loading, which showed the most uniform NiO particles.

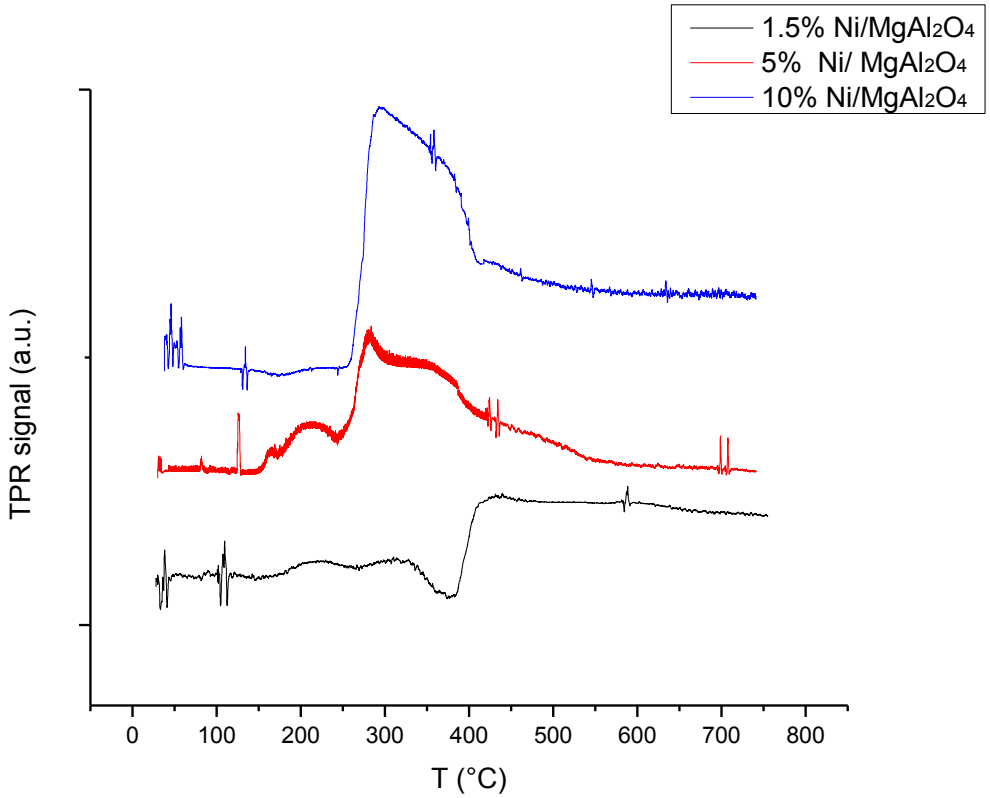


**Figure 10**: TPR profiles of the three catalysts.

### *3.6 - Characterisation of the spent samples*

The TPO analyses were carried out on the spent catalysts, to quantify both the nature (amorphous or ordered C, depending on the oxidation temperature) and their amount. The profiles show that C oxidation occurred at *ca*. 370 °C for sample 1.5% Ni/$MgAl_2O_4$ and 10% Ni/$MgAl_2O_4$ likely corresponding to amorphous carbon on Ni particles, while at *ca*. 538 °C for catalyst 5% Ni/ $MgAl_2O_4$ (Figure 11). This higher oxidation temperature and lower intensity can be ascribed to more structured C, such as the presence of graphitic layers. The quantification of C deposition is also reported in Table 7. The presence of structured C deposits is also confirmed by TEM and FE-SEM analysis, which evidence the presence of C nanotubes (Fig. 3,4) and by micro-RAMAN spectroscopy (Fig. 12). The latter presents for each sample the typical D and G bands usually found in the presence of multiwalled C nanotubes, with higher intensity for the highest Ni content.

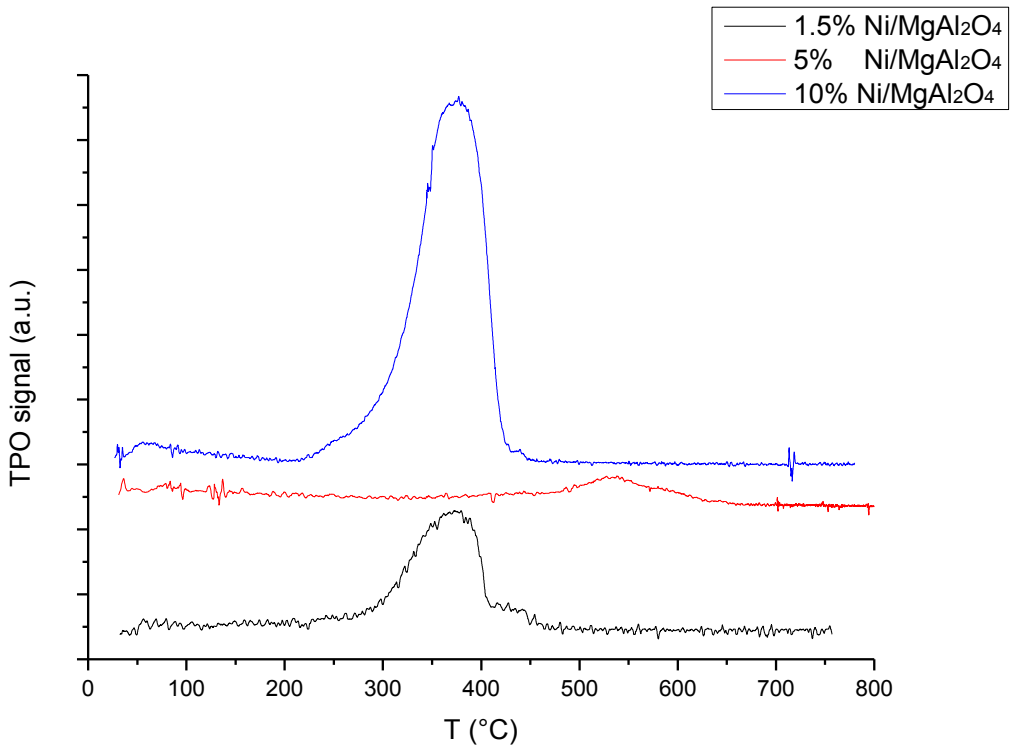


**Figure 11**: TPO profile of Ni catalysts.

**Table 7**: Mass of carbon per mass of spent catalyst expressed as %.

| **Sample** | **C wt%** |
|---|---|
| 1.5% $Ni/MgAl_2O_4$ | 6.58 |
| 5% $Ni/MgAl_2O_4$ | 5.29 |
| 10% $Ni/MgAl_2O_4$ | 14.86 |

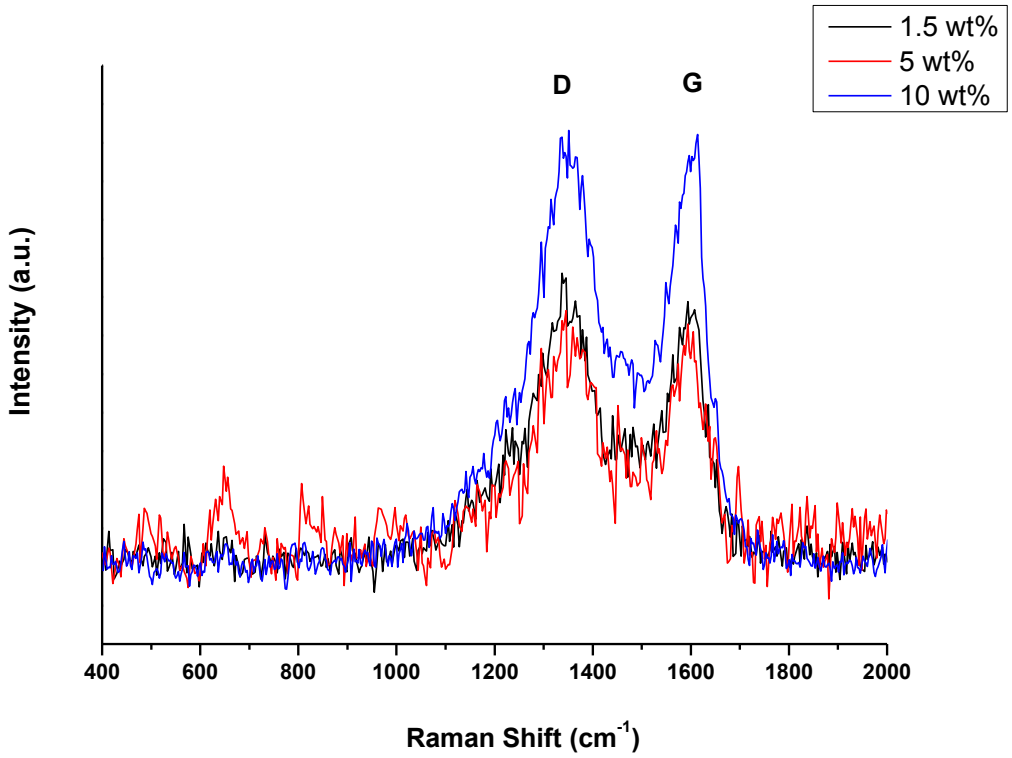


**Figure 12**: Micro-RAMAN spectra of used catalysts (last testing temperature = 400°C).

## *3.7 - General discussion*

Based on the negligible acidity of the support, the ethanol dehydration features are attributed only to Ni Lewis acidity. However, under the present conditions, limited effect of Ni coking was observed in the case of the lowest and highest Ni loading for different reasons. The amorphous coke characterizing both catalysts likely formed due to ethanol dehydration to ethylene during low temperature testing (400 °C). Reactivity for dehydration was quite limited due to small acidity (TPD of ammonia) in the case of 1.5 wt% Ni, whereas it was higher for 10 wt% Ni in virtue of its higher acidity, due to Ni particles. This form of coking is much more limited at higher reaction temperature due to consecutive reforming of the ethylene formed (if any), as testified by the products distribution. Furthermore, it can be tuned by increasing the water amount in the feed and is reversible by periodic regeneration

of the catalyst. Even if higher acidity of 10 wt% Ni could lead to higher ethylene formation, its higher C-C bond cleavage activity improved its further conversion to reformate.

On the other hand, the higher coke oxidation temperature observed in the case of 5 wt% Ni suggests a more structured carbon, usually in form of nanotubes. This implies a more critical failure of the catalyst, which brings to reactor fouling and to the physical detachment of the active phase from the support surface. This (limited) coke formation can be favored by NiO species poorly interacting with the support, likely being bigger particles, represented by the low temperature reduction feature in TPR analysis. The incorporation of part of Ni in the spinel phase for 10 wt% Ni observed by XPS and XRD analysis may improve its overall dispersion (even at such a high loading), thus preventing the formation of bigger Ni particles as in the case of 5 wt% Ni. The latter are involved in the formation of C nanotubes as previously discussed. These results confirm the effect of Ni dispersion, of its particle size and the interaction with the support in limiting the coking activity. This point has been already discussed in the literature [12-17,29,30,44-46].

On the basis of all the considerations above reported, 10 wt% Ni/$MgAl_2O_4$ represents an active and stable catalyst when tested at 625 °C. This operating temperature is lower than that usually applied to this reaction, in light of process intensification. The absence of intrinsic acidity of the support limits the deactivation phenomena by coking due to ethanol dehydration paths. However, a limited contribution to acidity is also attributed to Ni itself, increasing with Ni loading. Unfortunately, the catalyst with low Ni loading, favorable from the point of view of low Ni acidity and low coking rate, was insufficiently active for steam reforming, due to insufficient C-C bond cleavage activity.

On the other hand, the support plays a significant role in this reaction by contributing to steam activation, forming activated OH species and ensuring their mobility towards the active Ni particles to provide oxidizing moieties.

DRIFT analysis allowed to investigate and get insight into possible reaction mechanisms. The first reaction step seems the formation of acetaldehyde through ethanol dehydrogenation. This intermediate may decompose to methane and CO or further oxidise to carbonate, acetate and in general carboxylic species. The latter path seems favored over the present catalysts based on DRIFT analysis and on the very limited concentration of methane in the products distribution. This evolution mechanism of acetaldehyde may be favored by the basic character of the support, which stabilizes acidic functions such as carboxylic acids and $CO_2$.

As a general comparison with similar catalysts, Aupetre *et al.* [47] reported a Rh-Ni/$MgAl_2O_4$ catalyst leading to 100% ethanol conversion with 4.41 mol $H_2$/mol of ethanol, at 700°C, GHSV = 13,400 $h^{-1}$, with a more favourable water/ethanol ratio of 4 mol/mol than the stoichiometric ration here used.

Similarly, Olivares *et al.* [48] reported almost full ethanol conversion and ca. 4.7 mol $H_2$/mol of ethanol, over a Ni/$MgAl_2O_4$-$CeO_2$ catalyst at 650°C, W/F = 49 g min/mol, with a water/ethanol ratio of 5 mol/mol.

Szijjártó *et al*. [49] reported a kinetic study on Ni(Co,Ce)/$MgAl_2O_4$ with almost full ethanol conversion and *ca.* 55% $H_2$ yield, at 400°C, W/F = 1,333 g min/mol, with a water/ethanol ratio of 9 mol/mol. Accordingly, the present samples showed competitive with what reported in the literature. Indeed, comparable activity and hydrogen productivity was achieved without the addition of a noble/rare metals, by using a lower water/ethanol ratio and at relatively low temperature.

## *4 - Conclusions*

A series of Ni-based catalysts supported over $MgAl_2O_4$ have been prepared with small Ni crystallite size and high surface area thanks to an ultrasound assisted synthesis. Sufficiently dispersed Ni particles were obtained even at high Ni loading. The catalysts showed limited

acidity, essentially due to the presence of Ni, acidity increasing with its loading, responsible of the ethanol dehydration to ethylene at low temperature. Ethylene can be further reformed provided that sufficiently active Ni species are present, such as in the case of 10 wt% Ni.

Acetaldehyde was found as intermediate by DRIFT analysis, formed by ethanol dehydrogenation and further reformed. Its evolution follows an oxidative path rather than decomposition.

Coking of these samples was in general very limited, due to small acidity, which limits one of the possible coking modes, *i.e*. ethylene polymerisation. Some amorphous coke was found on the catalysts with the lowest and highest Ni loading, whereas the 5 wt% Ni sample was characterised by more structured carbon, which can be more critical as for regeneration.

Overall, 10 wt% Ni/$MgAl_2O_4$ proved active and sufficiently stable catalyst at 625 °C and even at 500 °C to represent a promising candidate for further optimisation of the process parameters.

## Acknowledgements

The valuable help of Dr. Matteo Compagnoni (Università degli Studi di Milano), Dr. James Carter (Cardiff University), Dr. Simon Kondrat (formerly Cardiff University, now Loughborough University) is gratefully acknowledged.

## References

[1] Park S, Vohs JM, Gorte RJ. Direct oxidation of hydrocarbons in a solid-oxide fuel cell. Nature**.** 2000;404:265–7. https://doi.org/10.1038/35005040.

[2] Baykara SZ. Hydrogen as fuel: a critical technology? Int. J. Hydrogen Energy**.** 2005;30:545–53. https://doi.org/10.1016/j.ijhydene.2004.06.010.

[3] Stiegel GJ, Ramezan M. Hydrogen from Coal Gasification: An Economical Pathway to a Sustainable Energy Future. Int. J. Coal. Geol. 2006;65:173-90. https://doi:10.1016/j.coal.2005.05.002.

[4] Le Valant A, Can F, Bion N, Duprez D, Epron F. Hydrogen production from raw bioethanol steam reforming: Optimization of catalyst composition with improved stability against various impurities. Int. J. Hydrogen Energy. 2010;35:5015-20. https://doi.org/10.1016/j.ijhydene.2009.09.008.

[5] Calles JA, Carrero A, Vizcaı´no AJ. Ce and La modification of mesoporous Cu–Ni/SBA-15 catalysts for hydrogen production through ethanol steam reforming. Microp. Mesop. Mater. 2009;119:200-7. https://doi.org/10.1016/j.micromeso.2008.10.028.

[6] Carrero A, Calles JA, Vizcaı´no AJ. Hydrogen production by ethanol steam reforming over Cu-Ni/SBA-15 supported catalysts prepared by direct synthesis and impregnation. Appl. Catal. A Gen. 2007;327:82-94. https://doi.org/10.1016/j.apcata.2007.04.030.

[7] Lindo M, Vizcaı´no AJ, Calles JA, Carrero A. Ethanol steam reforming on Ni/Al-SBA-15 catalysts: Effect of the aluminium content. Int. J. Hydrogen Energy. 2010;35:5895-901. https://doi.org/10.1016/j.ijhydene.2009.12.120.

[8] Haryanto A, Fernando S, Murali N, Adhikari S. Current Status of Hydrogen Production Techniques by Steam Reforming of Ethanol: A Review. Energy Fuels. 2005;19:2098-106. https://doi.org/10.1021/ef0500538.

[9] De Lima SM, Da Cruz IO, Jacobs G, Davis BH, Mattos LV, Noronha FB. Steam reforming, partial oxidation, and oxidative steam reforming of ethanol over Pt/CeZrO2 catalyst. J. Catal. 2008;257:356-68. https://doi.org/10.1016/j.jcat.2008.05.017.

[10] Pompeo F, Santori GF, Nichio NN. Hydrogen production by glycerol steam reforming with $Pt/SiO_2$ and $Ni/SiO_2$ catalysts. Catal. Today. 2011;172:183-8. https://doi.org/10.1016/j.cattod.2011.05.001.

[11] Wang F, Cai W, Provendier H, Schuurman Y, Descorme C, Mirodatos C, Shen W. Hydrogen production from ethanol steam reforming over Ir/$CeO_2$ catalysts: Enhanced stability by $PrO_x$ promotion. Int. J. Hydrogen Energy. 2011;36:13566-74. https://doi.org/10.1016/j.ijhydene.2011.07.091

[12] Nichele V, Signoretto M, Menegazzo F, Rossetti I, Cruciani G. Hydrogen production by ethanol steam reforming: Effect of the synthesis parameters on the activity of Ni/$TiO_2$ catalysts. Int. J. Hydrogen Energy. 2014;39:4252-8. https://doi.org/10.1016/j.ijhydene.2013.12.178.

[13] Rossetti I, Lasso J, Finocchio E, Ramis G, Nichele V, Signoretto M, Di Michele A. $TiO_2$-supported catalysts for the steam reforming of ethanol. Appl. Catal. A. 2014;477:42–53. https://doi.org/10.1016/j.apcata.2014.03.004.

[14] Finocchio E, Rossetti I, Ramis G. Redox properties of Co- and Cu-based catalysts for the steam reforming of ethanol. Int. J. Hydrogen Energy. 2013;38:3213-25. https://doi.org/10.1016/j.ijhydene.2012.12.137.

[15] Rossetti I, Lasso J, Finocchio E, Ramis G, Nichele V, Signoretto M, Di Michele A. Silica and zirconia supported catalysts for the low-temperature ethanol steam reforming. Appl. Catal. B. 2014;150-151:257-67. https://doi.org/10.1016/j.apcatb.2013.12.012.

[16] Compagnoni M, Lasso J, Di Michele A, Rossetti I, Flame-pyrolysis-prepared catalysts for the steam reforming of ethanol. Catal. Sci. & Technol. 2016;6:6247-56. https://doi.org10.1039/C5CY01958C.

[17] Rossetti I, Lasso J, Compagnoni M, Finocchio E, Ramis G, Di Michele A, Zucchini A, Dzwigaj S. Syngas production via steam reforming of bioethanol over Ni-BEA catalysts: A BTL strategy. Int. J. Hydrogen Energy. 2016;41:16878-89. https://doi.org/10.1016/j.ijhydene.2016.07.149.

[18] Vizcaı´no AJ, Carrero A, Calles JA. Hydrogen production by ethanol steam reforming over Cu–Ni supported catalysts. Int. J. Hydrogen Energy. 2007;32:1450-61. https://doi.org/10.1016/j.ijhydene.2006.10.024.

[19] Dave CD, Pant KK. Renewable hydrogen generation by steam reforming of glycerol over zirconia promoted ceria supported catalyst. Renewable Energy**.** 2011;36:3195-202. https://doi.org/10.1016/j.renene.2011.03.013.

[20] Denis A, Grzegorczyk W, Gac W, Machocki A. Steam reforming of ethanol over Ni/support catalysts for generation of hydrogen for fuel cell applications. Catal. Today. 2008;137:453-9. https://doi.org/10.1016/j.cattod.2008.03.006.

[21] Wen G, Xu Y, Ma H, Xu Z, Tian Z. Production of hydrogen by aqueous-phase reforming of glycerol. Int. J. Hydrogen Energy. 2008;33:6657-66. https://doi.org/10.1016/j.ijhydene.2008.07.072.

[22] Konsolakis M, Ioakimidis Z, Kraia T, Marnellos GE. Hydrogen Production by Ethanol Steam Reforming (ESR) over CeO2 Supported Transition Metal (Fe, Co, Ni, Cu) Catalysts: Insight into the Structure-Activity Relationship. Catalysts. 2016;6 (39):1-27. https://doi.org/10.3390/catal6030039.

[23] Compagnoni M, Tripodi A, Rossetti I. Parametric Study and Kinetic Testing for Ethanol Steam Reforming. Appl. Catal. B**.** 2017;203:899-909. https://ac.els-cdn.com/S0926337316308608/dx.doi.org/10.1016/j.apcatb.2016.11.002.

[24] Tripodi A, Compagnoni M, Rossetti I. Kinetic modeling and reactor simulation for ethanol steam reforming. ChemCatChem. 2016;8:3804-13. http://dx.doi.org/10.1002/cctc.201601075.

[25] Coleman LJI, Epling W, Hudgins RR, Croiset E. Ni/Mg–Al mixed oxide catalyst for the steam reforming of ethanol. Appl. Catal. A. 2009;363:52-63. https://doi.org/10.1016/j.apcata.2009.04.032.

[26] Trane-Restrupa R, Dahlb S, Jensen AD. Steam reforming of ethanol over Ni-based catalysts: Effect of feed composition on catalyst stability. Int. J. Hydrogen Energy. 2014;39:7735-46. https://doi.org/10.1016/j.ijhydene.2014.03.107.

[27] Katheria S, Deo G, Kunzru D. Washcoating of Ni/$MgAl_2O_4$ Catalyst on FeCralloy Monoliths for Steam Reforming of Methane. Energy Fuels. 2017;31(3):3143-53. https://doi.org/10.1021/acs.energyfuels.6b03423.

[28] Barroso MN, Galetti AE, Abello C. Ni catalysts supported over $MgAl_2O_4$ modified with Pr for hydrogen production from ethanol steam reforming. Appl. Catal. A 2011;394:124-31. http://doi.org/10.1016/j.apcata.2010.12.038.

[29] Rossetti I, Gallo A, Dal Santo V, Bianchi CL, Nichele V, Signoretto M, Finocchio E, Ramis G, Garbarino G, Di Michele A. Nickel catalysts supported over $TiO_2$, $SiO_2$ and $ZrO_2$ for the steam reforming of glycerol. ChemCatChem. 2013;5:294-306. http://doi.org/10.1002/cctc.201200481.

[30] Rossetti I, Biffi C, Bianchi CL, Nichele V, Signoretto M, Menegazzo F, Finocchio E, Ramis G, Di Michele A. Ni/$SiO_2$ and Ni/$ZrO_2$ catalysts for the steam reforming of ethanol. Appl. Catal. B. 2012:117-118:384-96. https://doi.org/10.1016/j.apcatb.2012.02.006.

[31] Mattos LV, Jacobs G, Davis BH, Noronha FB. Production of hydrogen from ethanol: Review of reaction mechanism and catalyst deactivation. Chem. Rev. 2012;112:4094-123. http://doi.org/10.1021/cr2000114.

[32] Centi G, Perathoner S. Opportunities and prospects in the chemical recycling of carbon dioxide to fuels. Catal. Today. 2009;48:191-205. https://doi.org/10.1016/j.cattod.2009.07.075.

[33] Chen D, Christensen KO, Ochoa-Fernández E, Yu Z, Tøtdal B, Latorre N, Monzón A, Holmen A. Synthesis of carbon nanofibers: effects of Ni crystal size during methane decomposition. J. Catal. 2005;229:82-96. https://doi.org/10.1016/j.jcat.2004.10.017.

[34] Christensen KO, Chen D, Lødeng R, Holmen A. Effect of supports and Ni crystal size on carbon formation and sintering during steam methane reforming. Appl. Catal. A. 2006;314:9-22. https://doi.org/10.1016/j.apcata.2006.07.028.

[35] Gonzalez De La Cruz VM, Holgado JP, Pereñíguez R, Caballero A. Morphology changes induced by strong metal–support interaction on a Ni–ceria catalytic system. J. Catal. 2008;257:307-14. https://doi.org/10.1016/j.jcat.2008.05.009.

[36] Grosvenor AP, Biesinger M, Smart R, McIntyre S. New interpretations of XPS spectra of nickel metal and oxides. Surface Science. 2006;600:1771-9. https://doi.org/10.1016/j.susc.2006.01.041.

[37] Biesinger MC, Payne BP, Grosvenor P, Lau WM, Gerson AG, Smart RStG. Resolving surface chemical states in XPS analysis of first row transition metals, oxides and hydroxides: Cr, Mn, Fe, Co and Ni. Applied Surface Science. 2011;257:2717-30. https://doi.org/10.1016/j.apsusc.2010.10.051.

[38] Velasquez Ochoa J, Trevisanut C, Millet JMM, Busca G, Cavani F. In situ DRIFTS-MS study of the anaerobic oxidation of ethanol over spinel mixed oxides. J. Phys. Chem. C. 2013;117:23908-18. https://doi.org/10.1021/jp409831t.

[39] Song H, Ozkan US. Ethanol steam reforming over Co-based catalysts: Role of oxygen mobility. J. Catal. 2009;261:66-74. https://doi.org/10.1016/j.jcat.2008.11.006.

[40] Song H, Zhang L, Watson RB, Braden D, Ozkan US. Investigation of bio-ethanol steam reforming over cobalt-based catalysts. Catalysis Today. 2007;129:346-54. https://doi.org/10.1016/j.cattod.2006.11.028.

[41] Llorca J, Homs N, Ramirez de la Piscina P. In situ DRIFT-mass spectrometry study of the ethanol steam-reforming reaction over carbonyl-derived Co/ZnO catalysts. J. Catal. 2004;227:556-60. https://doi.org/10.1016/j.jcat.2004.08.024.

[42] de Lima SM, da Silva AM, da Costa LOO, Assaf JM, Jacobs G, Davis BH, Mattos LV, Noronha FB. Evaluation of the performance of Ni/$La_2O_3$ catalyst prepared from $LaNiO_3$

perovskite-type oxides for the production of hydrogen through steam reforming and oxidative steam reforming of ethanol. Appl. Catal. A. 2010;377:181-90. https://doi.org/10.1016/j.apcata.2010.01.036.

[43] Rintramee K, Föttinger K, Rupprechter G, Wittayakun J. Ethanol adsorption and oxidation on bimetallic catalysts containing platinum and base metal oxide supported on MCM-41. Appl. Catal B. 2012;115-116:225-35. https://doi.org/10.1016/j.apcatb.2011.11.050.

[44] Palma V, Ruocco C, Meloni E, Ricca A. Highly active and stable Pt-Ni/$CeO_2$-$SiO_2$ catalysts for ethanol reforming. J. Clean. Prod. 2017;166:263-72. http://dx.doi.org/10.1016/j.jclepro.2017.08.036.

[45] Vizcaìno AJ, Lindo M, Carrero A, Calles JA. Hydrogen production by steam reforming of ethanol using Ni catalysts based on ternary mixed oxides prepared by coprecipitation. Int. J. Hydrogen Energy. 2012;37:1985-92. doi:10.1016/j.ijhydene.2011.04.179.

[46] Palma V, Ruocco C, Meloni E, Ricca A. Influence of Catalytic Formulation and Operative Conditions on Coke Deposition over CeO2-SiO2 Based Catalysts for Ethanol Reforming. Energies. 2017;10:1030-1042. doi:10.3390/en10071030.

[47] Aupretre F, Descorme C, Duprez D, Casanave D, Uzio D. Ethanol steam reforming over MgxNi1−xAl2O3 spinel oxide-supported Rh catalysts. J. Catal. 2005;233:464–77. doi:10.1016/j.jcat.2005.05.007.

[48] Villagrán Olivares AC, Gomez MF, Barroso MN, Abello MC. Ni-supported catalysts for ethanol steam reforming: effect of the solvent and metallic precursor in catalyst preparation, I.J.I.C. 2018;9:61–73. https://doi.org/10.1007/s40090-018-0135-6.

[49] Szijjártó GP, Pászti Z, Sajó I, Erdöhelyi A, Radnóczi G, Tompos A. Nature of the active sites in Ni/$MgAl_2O_4$-based catalysts designed for steam reforming of ethanol. J. Catal. 2013;305:290–306. http://dx.doi.org/10.1016/j.jcat.2013.05.036.